J. Electrochem. Sci. Eng. **10(1)** (2020) 21-28; http://dx.doi.org/10.5599/jese.708

Open Access: ISSN 1847-9286
www.jESE-online.org

Original scientific paper

Atomic layer deposited V_2O_5 coatings: a promising cathode for Li-ion batteries

Martyn Pemble[1,2], Ian Povey[1], Dimitra Vernardou[3,✉]

[1]*Tyndall National Institute, University College Cork, Lee Maltings, Prospect Row, Cork, Ireland*
[2]*School of Chemistry, University College Cork, Cork, Ireland*
[3]*Department of Electrical & Computer Engineering, School of Engineering, Hellenic Mediterranean University, 710 04 Heraklion, Crete, Greece*

Corresponding author: ✉dvernardou@staff.hmu.gr; Tel.: +30 2810 379753

Received: July 5, 2019; Revised: September 14, 2019; Accepted: September 25, 2019

Abstract

A modified, thermal atomic layer deposition process was employed for the pulsed chemical vapour deposition growth of vanadium pentoxide films using tetrakis (dimethylamino) vanadium and water as a co-reagent. Depositions were carried out at 350 °C for 400 pulsed CVD cycles, and samples were subsequently annealed for 1hour at 400 °C in air to form materials with enhanced cycling stability during the continuous lithium-ion intercalation/deintercalation processes. The diffusion coefficients were estimated to be 2.04×10^{-10} and 4.10×10^{-10} $cm^2\ s^{-1}$ for the cathodic and anodic processes, respectively. These values are comparable or lower than those reported in the literature, indicating the capability of Li^+ of getting access into the vanadium pentoxide framework at a fast rate. Overall, it presents a specific discharge capacity of 280 mA h g^{-1}, capacity retention of 75 % after 10000 scans, a coulombic efficiency of 100 % for the first scan, dropping to 85 % for the 10000th scan, and specific energy of 523 W h g^{-1}.

Keywords

Pulsed-CVD; vanadium pentoxide; Li^+ intercalation/deintercalation; cyclic voltammetry; cycling stability; electron transport properties

Introduction

The global energy crisis and growing ecological concerns have led to intensive development associated with energy use and environmental preservation [1]. For this reason, the need for clean and efficient energy storage has become paramount. New energy industries including electric vehicles (EVs) and hybrid electric vehicles (HEVs) need large scale energy storage systems (ESSs)

with advanced safety, high reliability, high energy density, high power density, low cost and minimal environmental impact [2].

Among the various ESSs, rechargeable lithium-ion batteries (LIBs) are the most promising candidates owing to their high energy density, long cycle lives and environmental friendliness [3]. Nevertheless, one of the key obstacles encountered in the commercialization of LIBs is the development of electrode materials. In particular, the determining factor for the overall energy density of LIBs is the capacity of the cathode, which is lower than that of the anode [4]. Hence, it is important to find cathodes with high reversibility, high rate capability and extended cycle stability.

Vanadium pentoxide (V_2O_5) is a well-known cathode material for LIBs due to its natural abundance, low cost, relatively easy synthesis and processing, and most importantly its high theoretical capacity of ≈ 440 mA h g^{-1} [5,6]. However, V_2O_5 in the bulk form suffers from poor rate capability and cycle stability due to its intrinsic structural instability and low Li^+ diffusivity (≈ 10^{-12} cm^2 s^{-1}) [7,8]. To address these issues, V_2O_5 has been synthesized into various nanostructures in order to improve the cycling performance and the rate capability [9-11]. V_2O_5 nanostructures offer many advantages [12] such as the short diffusion length facilitating the transport kinetics of electrons and Li^+. The small particle size and the large electrode/electrolyte contact area enhance the utilization of active materials accommodating more effectively the strain of Li intercalation/deintercalation.

This paper deals with the atomic layer deposition (ALD) for the growth of V_2O_5 as the cathode material. This method has several advantages [13] compared to other conventional thin-film deposition techniques, such as sol-gel, physical vapor deposition and chemical vapor deposition including the conformality, digital thickness control down to the sub-Å level, low substrate temperature, uniform and pinhole-free films and low impurity content.

The first application of ALD for LIBs was initially reported in 2000 [14]. Since then, there are several research papers dealing with ALD V_2O_5 as the cathode material. Crystalline V_2O_5 was readily obtained by ALD without any thermal post-treatment from vanadium (V) oxytri-isopropoxide [$VO(OC_3H_7)_3$, VTOP] and ozone (O_3) in a temperature window of 170-185 °C [15,16]. These films presented an initial specific discharge capacity of 147 mA h $g^{-1}$and capacity retention of 100 % after approximately 100 cycles. Additionally, α-V_2O_5 has been synthesized on carbon nanotubes (CNTs) by ALD presenting an initial specific discharge capacity of 450 mA h g^{-1}, which drops to approximately 200 mA h g^{-1} after 100 scans [17]. One can then observe that most studies have been focused on organic electrolytes, and rarely on aqueous electrolytes.

In this paper, we present the electrochemical performance of ALD V_2O_5 in an aqueous solution of 0.001 mol cm^{-3} LiCl showing excellent rate capability and cycling stability (capacity retention of 75 % after 10000 scans).

Experimental

Growth procedure

Thin films were deposited using a Cambridge-Nanotech Fiji ALD system on ITO coated glass substrates with a sheet resistance of 30-60 Ω/cm^2 (Sigma-Aldrich). Tetrakis (dimethylamino) vanadium (IV) ($V(NMe_2)_4$) (Strem US, min. 95 % TDMAV) and water were used as the vanadium source and co-reagent in a thermal ALD process. Depositions were carried out at 350 °C for 400 pulsed-CVD cycles using a nanolaminate method. Pulse durations for TDMAV and water were 300 and 100 ms respectively and all pulses were separated by 10 second purges. Samples were subsequently annealed for 1h at 400 °C in air. Further details of the film deposition method have previously been reported [18].

Characterization techniques

X-ray diffraction (XRD) was performed using a Rigaku (RINT 2000) diffractometer with Cu Kα for 2θ = 10.00-50.00°, a range of step sizes and time step 30 s/° for a glancing angle 0.5°. Raman measurements were performed with a Nicolet Almega XR micro-Raman system operating at wavenumber range 100-1100 cm^{-1} using a 473 nm laser. The morphology of the films was studied by scanning electron microscopy (SEM) with a FEI Quanta FEG 650 SEM and the surface elemental estimation was evaluated using energy dispersive X-ray spectroscopy (EDS) analysis in a Jeol JSM-7000 microscope.

Electrochemical evaluation of the samples was performed in a three-electrode cell as reported previously [19-22] using 0.001 mol cm^{-3} LiCl aqueous solution as an electrolyte for 10000 continuous Li^+ intercalation/deintercalation scans at 10 mV s^{-1}. The counter electrode was Pt, the working electrode was ALD V_2O_5 and all potential values were taken with respect to a standard Ag/AgCl reference electrode. The geometrical area of the working electrode (*i.e*. ALD samples) was 1 cm^2. Additionally, cyclic voltammograms were obtained at scan rates of 1.5, 5, 10, 20 and 50 mV s^{-1} for the diffusion coefficient estimation. Chronopotentiometric measurements were performed at a constant specific current of 450 mA g^{-1} and at potential ranging from -0.8 V to +1.0 V. Finally, electrochemical impedance spectroscopy (EIS) studies were obtained by PGSTAT302N, and the same instrument was used in all electrochemical measurements. Nyquist plots were acquired for the alternating current (AC) amplitude of 5.0 mA and set potential +0.3 V over the frequency range of 100 kHz to 10 mHz.

Results and discussion

Morphology

As shown in Figures 1 and 2, there is little to distinguish among the un-annealed and annealed samples, with the samples showing signs of some degree of texturing. EDS analysis confirms the presence of vanadium oxide (Figure 1 (c)). The thickness of V_2O_5 was estimated to be 22 **±** 3nm (Fig. 2).

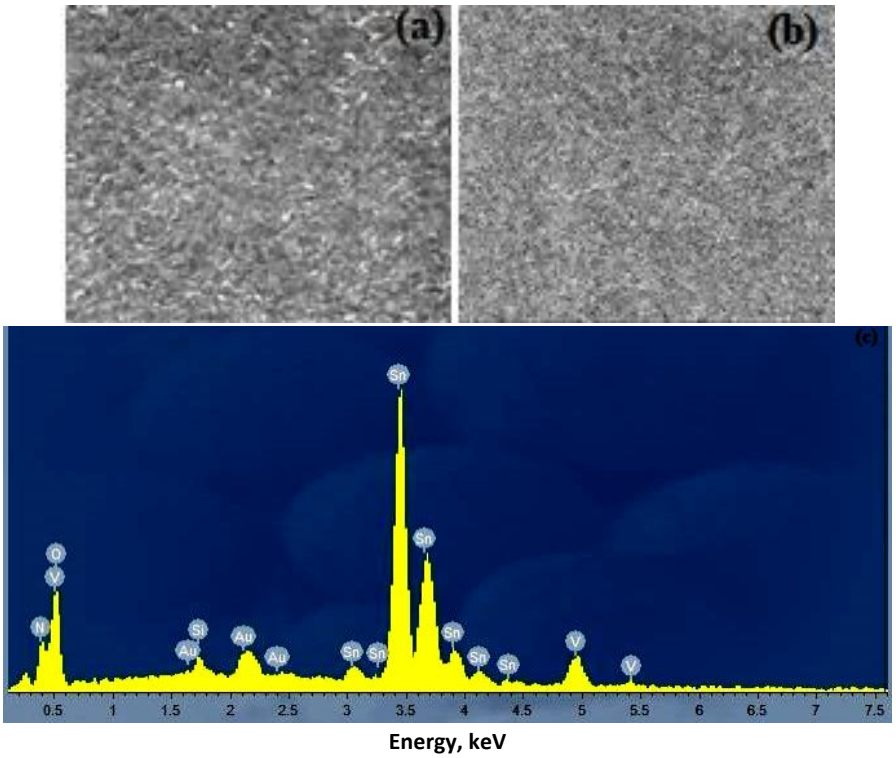

Figure 1. *SEM micrographs of un-annealed (a) and annealed at 400 °C for 1 h (b), V_2O_5 filmsfor a magnification ×50,000 and a bar equal with 2 µm. EDS spectrum for annealed V_2O_5 film (c)*

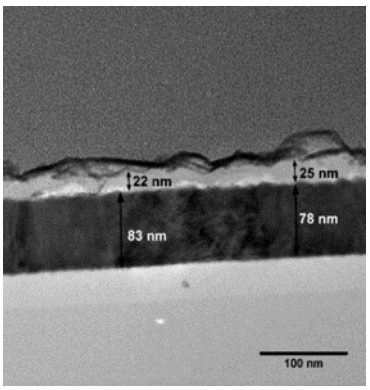

Figure 2. *Cross-sectional TEM micrographs of V_2O_5 film annealed at 400 °C for 1 hour (1 - V_2O_5; 2 - ITO surface layer of substrate)*

Structure

XRD patterns are presented in Figure 3(a). Films prepared by thermal ALD were amorphous 'as-grown' and a post annealing step was therefore required to produce crystalline films with enhanced stability. As shown in Figure 3, in the case of annealed V_2O_5 sample, three peaks assigned to orthorhombic α-V_2O_5 [7] were observed according with Joint Committee on Powder Diffraction Standard no. 41-1426. The intensity of the peaks is low due to the small thickness of V_2O_5 layer. Raman spectrum of the annealed V_2O_5 sample is in excellent agreement with that reported previously [23] (Figure 3(b)) indicating all characteristic vibrations with no shift.

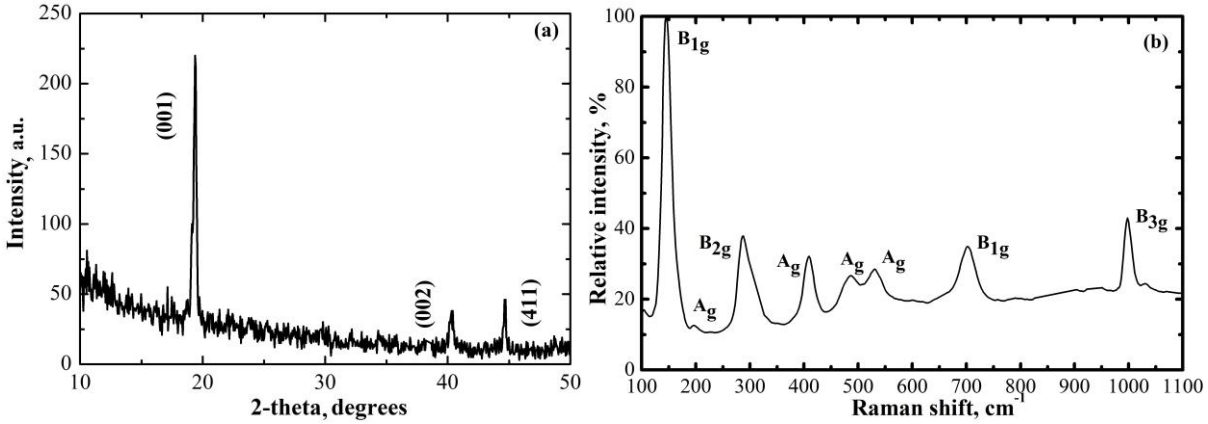

Figure 3*. XRD pattern (a) and Raman spectrum (b) of annealed V_2O_5 samples at 400 °C for 1 h*

Cyclic voltammetry

Cyclic voltammograms in the form of current density-potential curves are presented in Figure 4 in order to illustrate the stability and reversibility of the samples after sweeping the potential from -1 to +1 V and back for 10000 continuous Li^+ intercalation/deintercalation cycles. From Figure 4, it may be seen that the voltammogram consists of three cathodic peaks at +0.28 V, +0.04 V and -0.91 V, which were accompanied by a three-step color change of V_2O_5, yellow→lightblue→green, suggesting that V^{5+} is being reduced to V^{4+} and V^{3+}. The reverse reactions also take place, as indicated by three corresponding anodic peaks at -0.47, +0.37 and +0.54 V. The current density was found to decrease from 0.5 mA cm^{-2} (first scan) to 0.25 mA cm^{-2} (2500^{th} scan) and remained constant afterwards, indicating the prolonged stability of the electrode as supported by the voltammograms showing no evidence of degradation after cycling for 10000 times. The sample presents enhanced electrochemical activity as compared with the literature [24,25].

It was not possible to study the electrochemical performance of the 'as-grown' V_2O_5 for more than five scan numbers because it fell apart in the electrolyte due to the poor stability.

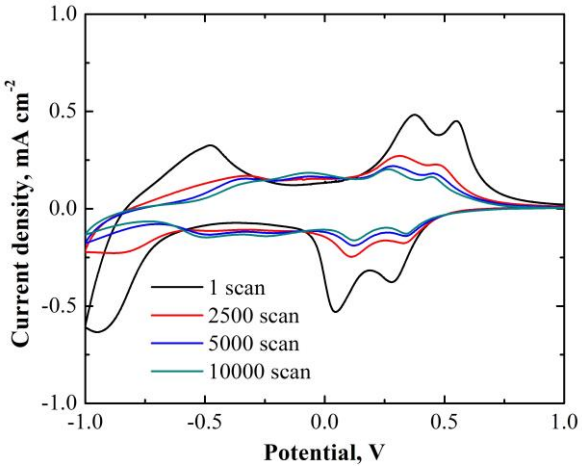

Figure 4. *Cyclic voltammograms displayed as current density vs. potential curves of V_2O_5 film, scan rate of 10 mV s^{-1} and varying number of continuous Li^+ intercalation/deintercalation scans up to 10000. The electrolyte utilized in all cases was 0.001 mol cm^{-3} LiCl aqueous solution*

Cyclic voltammograms recorded at different scan rates are presented in Figure 5(a). From Figure 5(a), it may be seen that the peak current increases with scan rate, while the shape of the curves is essentially retained suggesting the operation of fast Li^+ intercalation/deintercalation reactions [26]. Furthermore, a linear relationship is obtained from the plot of peak current density as a function of the square root of scan rate suggesting diffusion-controlled processes (Figure 5(b)). The Li^+ diffusion coefficient can be estimated according to equations (1) and (2) which, however, should be taken with certain reserve [20]:

$$I_p = D^{1/2}\, 2.72\times10^5\, n^{3/2} A C v^{1/2} \quad (1)$$

$$D^{1/2} = \frac{a}{2.72\times10^5\, n^{3/2} A C} \quad (2)$$

In eqs. (1)and (2), I_p is the peak (anodic and cathodic) current, A; D is the diffusion coefficient, $cm^2\ s^{-1}$; n is the number of electrons; A is the crosssectionalarea, cm^2; C is the concentration of Li^+, mol cm^{-3}; v is the scan rate, V s^{-1} and a is the slope obtained from Figure 5(b). In this study A and n have unity values, while C was declared to be 0.001 in equation (2). The diffusion coefficient was found to be 2.04×10^{-10} and 4.10×10^{-10} $cm^2\ s^{-1}$ for the cathodic and anodic processes, respectively. By comparison with the values taken from the literature in Table 1, it may be concluded that the V_2O_5 films produced in this work show comparable or lower diffusion coefficients as compared with other materials.

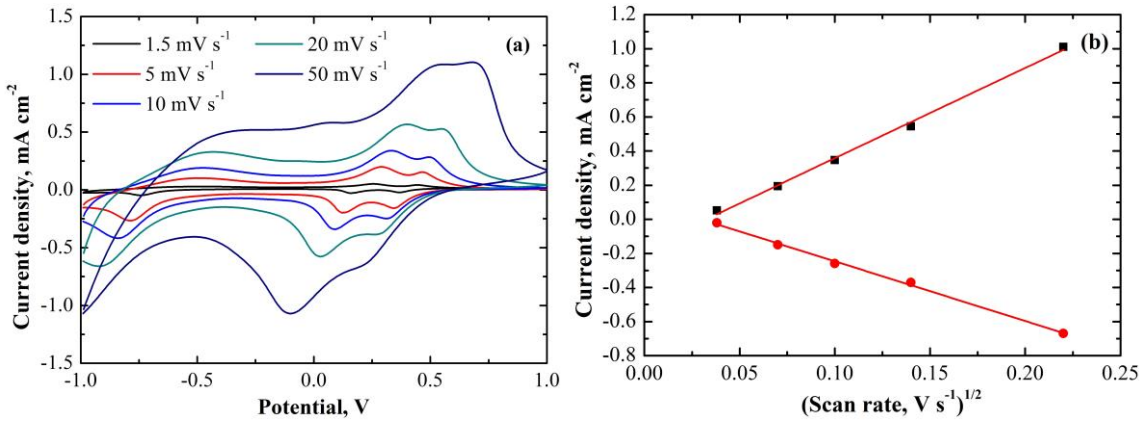

Figure 5. *Cyclic voltammograms displayed as current density vs. potential curves of the annealed V_2O_5 film recorded at 1.5, 5, 10, 20 and 50 mV s^{-1} (a). Anodic (squares) and cathodic (circles) peak current density values as a function of the square root of scan rate (the fitting is also indicated) (b)*

Table 1: *Diffusion coefficient values of other materials in aqueous electrolytestaken from the literature.*

Material	Diffusion coefficient, cm^2s^{-1}	Reference
3D-printed graphene	1.91×10^{-7}	[19]
MnO_2	0.882×10^{-11}	[20]
nanorutile TiO_2	7.0×10^{-8}	[27]
nano-CaO-SnO_2	1.0×10^{-14}	[28]
Cs_4PbBr_6	7.34×10^{-8}	[29]
V_2O_5	4.10×10^{-10}	This work

The chronopotentiometric curves of V_2O_5 films under the constant specific current of 450 mA g^{-1} and potential ranging from -0.8 V to +1.0 V *vs*. Ag/AgCl are presented in Figure 6(a). It is indicated that the discharging process shows three plateau regions at approximately -0.64 V, +0.17 and +0.37 V indicating the three-step process as also observed in cyclic voltammetry analysis. The specific discharge capacity reported for V_2O_5 is found to be 280 mA h g^{-1} with capacity retention of 75 % after 10000 scans, which is comparable with others reported in the literature*, i.e.* 140 [16], 350 [17] and 368 mA h g^{-1} [30] with a capacity retention close to 100 % for shorter scan numbers as compared with our work. Nevertheless, Figure 6(b) presents the trend of specific discharge capacity as a function ofthe scan number. The continuous Li^+ intercalation/deintercalation processes cause dissolution of V_2O_5 film resulting in the fading of discharge capacity from the first to the 2500th scan, which however remains stable enough for 10000 scans. Additionally, Figure 6(b) indicates the coulombic efficiency as estimated from the specific discharge capacity divided by the specific charge capacity. It is found to be 100 % for the first scan,dropping to 85 % for the 10000th scan.

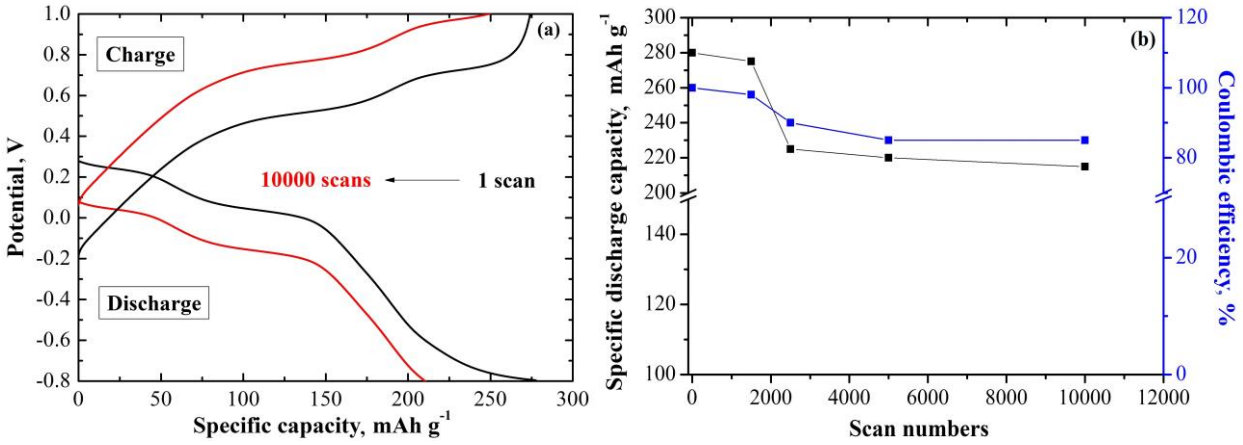

Figure 6. *Chronopotentiometric curves for V_2O_5 film under specific current of 450 mA g^{-1} and potential ranging from -0.8 V to +1.0 V (a). Specific discharge capacity and coulombic efficiency as a function of the scan numbers (b)*

The specific discharge capacity was evaluated at different specific currents ranging from 450 mA g^{-1} to 1500 mA g^{-1} (Figure 7(a)). It is shown that the specific discharge capacity drops to 225 mA h g^{-1} at the highest specific current (1500 mA h g^{-1}), presenting retention of 80 %. Furthermore, the cathode can still deliver a specific discharge capacity of 278 mA h g^{-1}, when the specific current returned to 450 mA g^{-1}, showing good structural stability.

Nyquist plots consist of semicircles in high-frequency regions and sloped lines in low-frequency regions (Figure 7 (b)). These correspond to the charge transfer resistance at the ALD V_2O_5 cathode/electrolyte interface and Warburg impedance associated with Li-ion diffusion in V_2O_5. The

plots were fitted based on a circuit mentioned elsewhere [29]. The charge transfer resistance from the 1st (5 Ω) to the 10000th scan (12 Ω) endow the sustainable performance of the ALD V_2O_5.

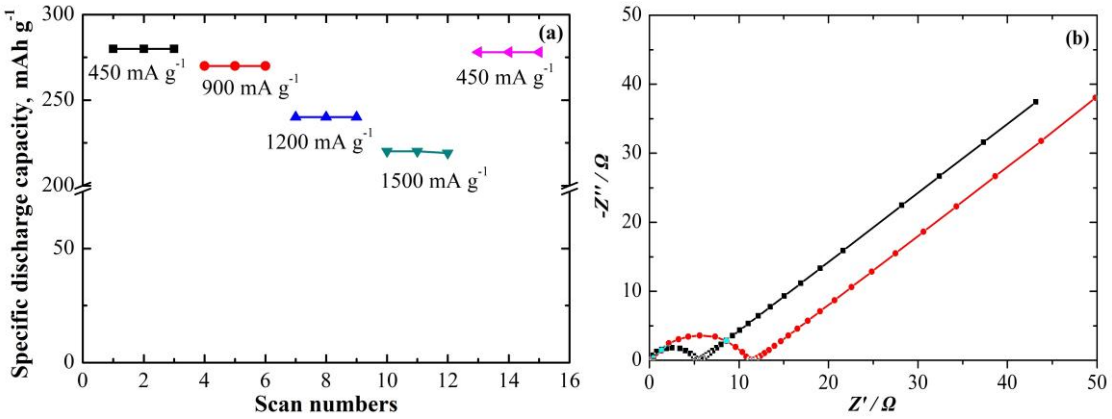

Figure 7. *Rate capability of V_2O_5 film at specific current ranging from 450 mA g^{-1} to 1500 mA g^{-1} and then back to 450 mA g^{-1} (a). Electrochemical impedance spectra of the first scan (black) and the 10000th scan (red) (b).*

Conclusions

A thermal ALD process for growth of V_2O_5 films was developed using tetrakis (dimethylamino) vanadium and water as a co-reagent. The process was subsequently modified in order to anneal V_2O_5 films with the aim of increasing stability of films on the substrate. Dense, uniform, crack-free crystalline films were produced. The diffusion coefficient was 2.04×10^{-10} and 4.10×10^{-10} cm^2 s^{-1} for the cathodic and anodic processes, respectively, allowing Li^+ access into V_2O_5 at a fast rate. Overall, the ALD V_2O_5 is a promising cathode for LIBS because it combines useful characteristics such as good stability, high specific discharge capacity of 280 mA h g^{-1} with capacity retention of 75 % and coulombic efficiency of 85 % after 10000 scans, high specific energy of 523 W h g^{-1} and ease of electron transport. The dissolution of V_2O_5 is a problem in the initial scans, which is restrained for longer periods benefiting this material as an electrode in LIBs.

Acknowledgements: *The support of Science Foundation Ireland Principal Investigator Grant, DEPO-Man (15/IA/3015) is gratefully acknowledged.*

References

[1] G. Cai, X. Wang, M. Cui, P. Darmawan, J. Wang, A. L. -S. Eh, P. S. Lee, *Nano Energy* **12** (2015) 258-267.
[2] P. Rüetschi, *Journal of Power Sources* **42** (1993) 1-7.
[3] B. Xu, D. Qian, Z. Wang, Y. S. Meng, *Materials Science and Engineering: Reports* **73** (2012) 51-65.
[4] D-J. Yan, X–D. Zhu, K–X. Wang, X–T. Gao, Y–J. Feng, K–N. Sun, Y–T. Liu, *Journal of Materials Chemistry A* **4** (2016) 4900-4907.
[5] Y. Wang, G. Cao, *Advanced Materials* **20** (2008) 2251-2269.
[6] J. Liu, H. Xia, D. Xue, L. Lu, *Journal of the American Chemical Society* **131** (2009) 12086-12087.
[7] S–H. Ng, T. J.Patey, R.Buchel, F. Krumeich, J–Z. Wang, H–K. Liu, S. E. Pratsinis, P. Novák, *Physical Chemistry Chemical Physics* **11** (2009) 3748-3755.
[8] Y. Wei, C–W. Ryu, K–B. Kim, *Journal of Power Sources* **165** (2007) 386-392.
[9] D. W. Su, S. X. Dou, G. X. Wang, *Journal of Materials Chemistry A* **2**(2014) 11185-11194.
[10] W. Cheng, G. Zeng, M. Niederberger, *Journal of Materials Chemistry A* **3** (2015) 2861-2868.
[11] G. Li, Y. Qiu, Y. Hou, H. Li, L. Zhou, H. Deng, Y. Zhang, *Journal of Materials Chemistry A* **3** (2015) 1103-1109.
[12] A. Manthiram, A. Vadivel Murugan, A. Sarkar, T. Muraliganth, *Energy Environmental Science* **1** (2008) 621-638.

[13] F. Mattelaer, K. Geryl, G. Rampelberg, T. Dobbelaere, J. Dendooven, C. Detavernier, *RSC Advances* **6** (2016) 11465-114665.
[14] J. C. Badot, S. Ribes, E. B. Yousfi, V. Vivier, J. P. Pereira-Ramos, N. Baffier, D. Lincot, *Electrochemical and Solid-State Letters* **3** (2000) 485-488.
[15] X. Chen, H. Zhu, Y–C. Chen, Y. Shang, A. Cao, L. Hu, G. W. Rubloff, *ACS Nano* **6** (2012) 7948-7955.
[16] X. Chen, E. Pomerantseva, P. Banerjee, K. Gregorczyk, R. Ghodssi, G. Rubloff, *Chemistry of Materials* **24** (2012) 1255-1261.
[17] M. Xie, X. Sun, H. Sun, T.Porcelli, S. M. George, Y. Zhou, J. Lian, *Journal of Materials Chemistry A* **4** (2016) 537-544.
[18] I. I. Kazadojev, S. O'Brien, L. P. Ryan, M. Modreanu, P. Osiceanu, S. Somacescu, D. Vernardou, M. E. Pemble, I. M. Povey, *ECS Transactions* **85** (2018) 83-94.
[19] D. Vernardou, K. C. Vasilopoulos, G. Kenanakis, *Applied Physics A* **123** (2017) 623-627.
[20] D. Vernardou, A. Kazas, M. Apostolopoulou, N. Katsarakis, E. Koudoumas, *Journal of Electronic Materials* **46** (2017) 2232-2240.
[21] D. Vernardou, I. Marathianou, N. Katsarakis, E. Koudoumas, I. I.Kazadojev, S. O'Brien, M. E. Pemble, I. M. Povey, *Electrochimica Acta* **196** (2016) 294-299.
[22] C. Drosos, C. Jia, S. Mathew, R. G. Palgrave, B. Moss, A. Kafizas, D. Vernardou, *Journal of Power Sources* **384** (2018) 355-359.
[23] M. Panagopoulou, D. Vernardou, E. Koudoumas, N. Katsarakis, D. Tsoukalas, Y. S. Raptis, *Journal of Physical Chemistry C* **121** (2017) 70-79.
[24] T. M. Westphal, C. M. Cholant, C. F. Azevedo, E. A. Moura, D. L. da Silva, R. M. J. Lemos, A. Pawlicka, A. Gündel, W. H. Flores, C. O. Avellaneda, *Journal of Electroanalytical Chemistry* **790** (2017) 50-56.
[25] Z. Tong, J. Hao, K. Zhang, J. Zhao, B–L. Su, Y. Li, *Journal of Materials Chemistry C* **2** (2014) 3651-3658.
[26] H. Yu, X. Rui, H. Tan, J. Chen, X. Huang, C. Xu, W. Liu, D. Y. W. Yu, H. H. Hng, H. E.Hoster, Q. Yan, *Nanoscale* **5** (2013) 4937-4943.
[27] S. Bach, J. P. Pereira-Ramos, P. Williams, *Electrochimica Acta* **55** (2010) 4952-4959.
[28] N. Sharma, K. M. Shaju, G. V. S. Rao, B. V. R. Chowdari, *Journal of Power Sources* **139** (2005) 250-260.
[29] A. Kostopoulou, D. Vernardou, K. Savva, E. Stratakis, *Nanoscale* **11** (2019) 882-889.
[30] X. Chen, E. Pomerantseva, K. Gregorczyk, R. Ghodssr, G. Rubloff, *RSC Advances* **3** (2013) 4294-4302.